



A discrete time evolution model for fracture networks

Gábor Domokos^{1,2} · Krisztina Regős^{1,2}

Accepted: 8 December 2022 / Published online: 29 December 2022
© The Author(s) 2022

Abstract

We examine geological crack patterns using the mean field theory of convex mosaics. We assign the pair (\bar{n}^*, \bar{v}^*) of *average corner degrees* (Domokos et al. in A two-vertex theorem for normal tilings. *Aequat Math* <https://doi.org/10.1007/s00010-022-00888-0>, 2022) to each crack pattern and we define two local, random evolutionary steps R_0 and R_1 , corresponding to secondary fracture and rearrangement of cracks, respectively. Random sequences of these steps result in trajectories on the (\bar{n}^*, \bar{v}^*) plane. We prove the existence of limit points for several types of trajectories. Also, we prove that *cell density* $\bar{\rho} = \frac{\bar{v}^*}{\bar{n}^*}$ increases monotonically under any admissible trajectory.

Keywords Fracture network · Evolution model · Discrete dynamical system · Evolution model · Tessellation

1 Introduction

Fragmentation is one of the most ubiquitous natural processes and the efforts to decode its geometry have been at the forefront of geological research (Adler and Thovert 1999; Domokos et al. 2020; Goehring and Morris 2008; Goehring 2013; Steacy and Sammis 1991; Nagle-McNaughton 2021; Ma et al. 2019; Aydin and DeGraff 1988; Garcia-Rodriguez 2015; Jagla and Rojo 2002; Turcotte 1986; Peacock et al. 2018). While many aspects of fragmentation are inherently three dimensional, the 2D aspects of the phenomenon are interesting in their own right: the most visible fingerprints of fragmentation are surface fracture patterns (also called 2D fracture networks) on various scales (Goehring 2013; Turcotte 1986), ranging from mud cracks resulting

✉ Gábor Domokos
domokos@iit.bme.hu

¹ Department of Morphology and Geometric Modeling, Budapest University of Technology and Economics, Műegyetem Rkp 3., K220, Budapest 1111, Hungary

² MTA-BME Morphodynamics Research Group, Budapest University of Technology and Economics, Műegyetem Rkp 3., K220, Budapest 1111, Hungary

from desiccation (Nagle-McNaughton 2021; Goehring 2013; Ma et al. 2019) (see Fig. 1 for two examples) through basalt columns (Goehring and Morris 2008; Jagla and Rojo 2002) to the pattern defined by the tectonic plates (Domokos et al. 2020; Bird 2003). The most common model for planar fracture geometry appear to be polygonal patterns (Aydin and DeGraff 1988; Garcia-Rodriguez 2015). In (Domokos et al. 2020) the geometric theory of tilings (Grünbaum and Shepard 1987; Schattschneider and Senechal 2004), in particular, the mean field theory of convex mosaics (Bird 2003; Schneider and Weil 2008) was applied to identify fracture networks with a point on the so-called symbolic plane, spanned by two characteristic geometric features, the *nodal and cell degrees* (Domokos and Lángi 2019; Schattschneider and Senechal 2004) (see Definitions 4 and 5 in Sect. 2).

However, fracture networks are not static objects; they *evolve* in various manners.

Evolution models are popular mathematical tools, used also in operations research (Vrankic et al. 2021). This particular evolution may be modeled by regarding an initial fracture network (to which we will refer as *primary network*) and then consider a family of discrete, local events under the random sequence of which the primary network evolves. While these events have been described in Domokos et al. (2020), the evolution model has not been developed and this is the goal of the current paper. Such a model would, for example, admit the following

Question 1 Could the pattern in Fig. 1a have evolved from the pattern in Fig. 1b or vice versa?

After constructing our model in Sects. 2 and 3, we will address Question 1 in Sect. 4, showing that the (a) \rightarrow (b) evolution is not admissible in the model but the (b) \rightarrow (a) is.

In the model we will consider two types of local events which evolve the fracture network. One such local event is undoubtedly *secondary fracture* where an existing fragment particle (produced in primary fracture) is being split into two parts along a (random) fracture line; this can be observed on rock outcrops. Another local event is when, in the process of crack healing and rearrangement “T” nodes evolve into “Y”

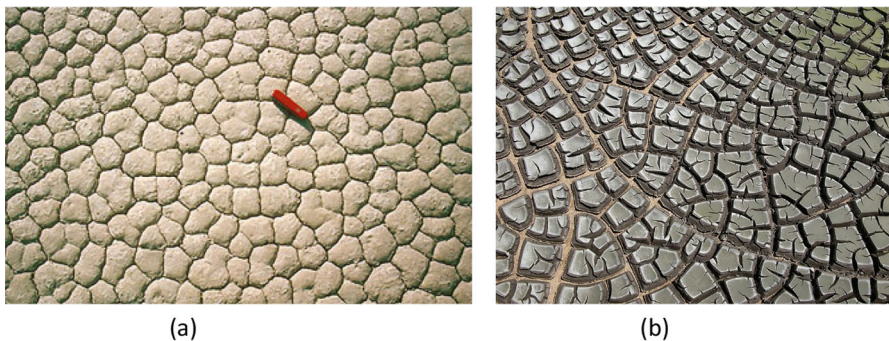


Fig. 1 Desiccation crack patterns in mud, also discussed in Domokos et al. (2020). Observe different geometric tiling patterns. Photo credit: **a** Charles E. Jones University of Pittsburgh, Pittsburgh, PA **b** Hannes Grobe, Alfred Wegener Institute, Bremerhaven, Germany

nodes; this can be observed in drying mud and also in columnar joints (Goehring 2013; Goehring and Morris 2008).

Our evolution model will only consider these two steps. Needless to say, the model could be refined by considering other local events. However, even this simple model suffices to show the principles of how such models operate in general and, as we will show, the model based on these two steps is already rich in dynamics and promises to explain several features of the observed natural processes.

Our paper is structured as follows: in Sect. 2 we introduce all necessary mathematical concepts. Section 3 is dedicated to the development of the model and the main results and in Sect. 4 we draw conclusions.

2 Mathematical concepts

As models of 2D fracture networks we consider *convex, normal tilings* which we define below, following (Domokos and Lángi 2019; Schneider and Weil 2008):

Definition 1 Normal tilings are 2 dimensional tessellations where each cell is a topological disk, the intersection of each of the two cells is either a connected set, or the empty set and the cells are uniformly bounded from below and above.

Definition 2 Convex tilings are 2 dimensional tessellations where each cell is convex.

Remark 1 As a direct consequence of Definitions 1 and 2, we see immediately that all cells of normal, convex tilings of the Euclidean plane are finite, convex polygons (see also (Domokos and Lángi 2019).) We can also see that normal tilings of infinite domains (such as the Euclidean plane) have infinitely many cells while normal tilings of finite (compact) domains have a finite number of cells.

Definition 3 A node of a convex, normal tiling is a point where at least 3 cells overlap.

Remark 2 As a consequence of Remark 1 and Definition 3, we can see that in a convex, normal tiling the boundary of each cell contains at least 3 nodes.

Definition 4 In a normal, convex tiling the combinatorial degree v of a cell is equal to the number of nodes on its boundary and the combinatorial degree n of a node is equal to the number of cells overlapping at that node.

Following (Domokos et al. 2022), we also introduce a concept, which is more sensitive to the actual shape of the cells:

Definition 5 In a normal, convex tiling the corner degree v^* of a cell is equal to the number of its vertices and the corner degree n^* of a node is equal to the number of vertices overlapping at that node (Fig. 2).

Remark 3 We can immediately see that for all cells and nodes we have $v^* \leq v$, $n^* \leq n$.

Definition 6 We call a node regular if $n^* = n$. We call a normal, convex tiling regular if all nodes are regular. We denote the number of all nodes by V and the number of

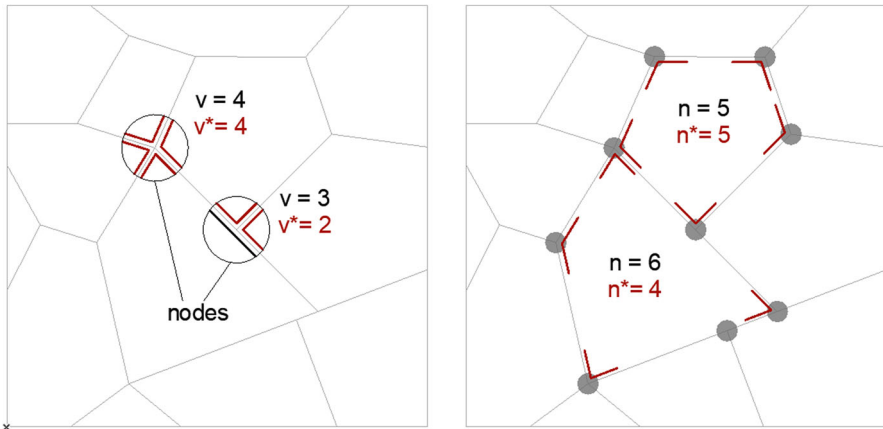


Fig. 2 Illustration of the basic geometrical concepts introduced in Definitions 3, 4 and 5: Combinatorial nodal and cell degrees n, v and corner degrees n^*, v^*

irregular nodes by V_I and the quantity $r = \frac{v - V_I}{v}$ is called the regularity of the tiling, $r = 1$ corresponding to regular tilings. (We remark that for regular tilings we have $v^* = v$ for all cells. We also see that for regular nodes we have $n^* \geq 3$ whereas for irregular nodes we have $n^* \geq 2$.)

The quantities v, v^*, n, n^* can be easily averaged on finite mosaics:

Definition 7 Let us denote the number of faces (cells), edges and vertices (nodes) of a finite portion of a convex, balanced tiling by F, E, V , respectively. We call the quantities

$$\bar{n} = \frac{N_V}{V} \tag{1}$$

$$\bar{v} = \frac{N_F}{F} \tag{2}$$

the combinatorial degrees of the tiling, where $N_F = \sum_{i=1}^F v_i; N_V = \sum_{i=1}^V n_i$ and n_i, v_i denote the combinatorial degrees of the i th node and cell, respectively. Similarly, the quantities

$$\bar{n}^* = \frac{N_V^*}{V} \tag{3}$$

$$\bar{v}^* = \frac{N_F^*}{F} \tag{4}$$

are called the corner degrees of the tiling, where $N_F^* = \sum_{i=1}^F v_i^*; N_V^* = \sum_{i=1}^V n_i^*$. We remark that N_F, N_V and N_F^*, N_V^* will only differ due to boundary terms. In our model (Hypothesis 1(B), Sect. 3) we will assume that the steps driving the evolution

occur in the interior of the pattern, so the evolution of N_F, N_V and N_F^*, N_V^* will be identical. For simplicity of notation we will drop the subscripts and we will refer to F, V, N, N^* as the fundamental quantities of the tiling.

The average degrees can also be defined for infinite normal tilings:

Definition 8 Select a sphere $B(X, \rho)$ with center X and radius ρ , and calculate the averages $\bar{n}(X, \rho), \bar{v}(X, \rho)$ and $\bar{n}^*(X, \rho), \bar{v}^*(X, \rho)$. The radius ρ is then increased to infinity. We say that the averages $\bar{n}, \bar{v}, \bar{n}^*$ and \bar{v}^* of the combinatorial and corner degrees exist if the limits $\lim_{\rho \rightarrow \infty} \bar{n}(X, \rho), \lim_{\rho \rightarrow \infty} \bar{v}(X, \rho), \lim_{\rho \rightarrow \infty} \bar{n}^*(X, \rho)$ and $\lim_{\rho \rightarrow \infty} \bar{v}^*(X, \rho)$ exist and they are independent from X . Tilings with property are called *balanced* (Grünbaum and Shepard 1987) tilings.

Remark 4 Henceforth we only consider normal, convex tilings and for all infinite tilings we require that they are balanced.

Definition 9 The $[\bar{n}, \bar{v}]$ plane is called the (*combinatorial*) *symbolic plane* and the $[\bar{n}^*, \bar{v}^*]$ plane is called the (*metric*) *symbolic plane*.

Remark 5 Based on Domokos and Lángi (2019) and Schneider and Weil (2008), for infinite, balanced, convex (a) regular and (b) irregular tilings of the Euclidean plane we have:

$$(a) \bar{v} = \frac{2\bar{n}}{\bar{n} - 2} \quad (b) \bar{v} = \frac{2\bar{n}}{\bar{n} - r - 1} \tag{5}$$

and there exist no infinite tilings for $\bar{v} > \frac{2\bar{n}}{\bar{n}-2}$ and no convex tilings for $\bar{v} > 2\bar{n}$.

Definition 10 Let M be a finite part of a regular, normal, convex tiling and let M have F faces (cells) and V vertices (nodes). Then we call $\bar{\rho}(M) = \frac{V}{F}$ the *cell density* of M . For infinite tilings we use the limit process described in Definition 6.

Remark 6 We can immediately see that $\bar{\rho}(M) = \frac{\bar{v}(M)}{\bar{n}(M)} = \frac{\bar{v}^*(M)}{\bar{n}^*(M)}$. So, the cell density can be expressed by the average cell degree and average nodal degree, but its value is *independent of the definition of these degrees*. We can also see that $\bar{\rho}(M) = \text{constant}$ lines correspond to rays passing through the origin of the symbolic plane.

3 An evolution model for fracture networks

Our model is inspired by Domokos et al. (2020), where planar fracture patterns have been analyzed and classified in the symbolic plane, based on their nodal and cell averages. The theory presented in Domokos et al. (2020) also gives a clue how *primary crack networks* emerge and what their geometrical properties are. Although this is not the subject of the current paper, we remark that, according to Domokos et al. (2020), one dominant mechanism for global primary crack networks are deformations under shear and this produces regular mosaics with averages close to $(\bar{n}^*, \bar{v}^*) = (4, 4)$. Here

we take one further step and build a model to study not only their current state but also their evolution in the symbolic plane.

We start by defining our main hypothesis. While we believe that this hypothesis captures several aspects of physical fragmentation, our goal is not just to define this particular evolution model but also to demonstrate how such a model is constructed and how it operates.

Hypothesis 1

- (A) The fracture network is a finite domain of a convex, balanced tiling of the Euclidean plane.
- (B) Evolution of the crack pattern takes place in a series of discrete events in the interior of the crack pattern. These events consist of 2 step-types (R_0, R_1) to be detailed below. The order of the step-types is important: we assume that the first k pieces of R_1 steps are preceded by at least $(k/2)$ pieces of R_0 steps. (This is explained in detail below when we define step R_1 .)
- (C) 1. During *secondary cracking*, one cell of the primary crack network is split into two parts along a straight line segment, connecting two points belonging to the relative interior of two different edges of the cell. (R_0 type step). *It is easy to see that R_0 type steps retain the convexity of the initial mosaic.* See Fig. 3.
2. (2) During *crack healing-rearrangement*, the edges and nodes of the crack network are rearranged so that “T” nodes evolve into “Y” nodes (Goehring 2013) and each such event corresponds to an R_1 -type step. Obviously, this step can only be performed on an irregular “T” node. Since we assumed the initial mosaic to be regular and one step of type R_0 generates two irregular nodes, the first k pieces of R_1 steps must be preceded by at least $(k/2)$ pieces of R_0 steps. See Fig. 3.

For clarity, below we summarize in Table 1 how the steps R_0 and R_1 operate on the fundamental quantities F, V, N, N^* of the tiling. Since we evolve the tiling in discrete steps and we introduce the serial number k of the step as a subscript to the

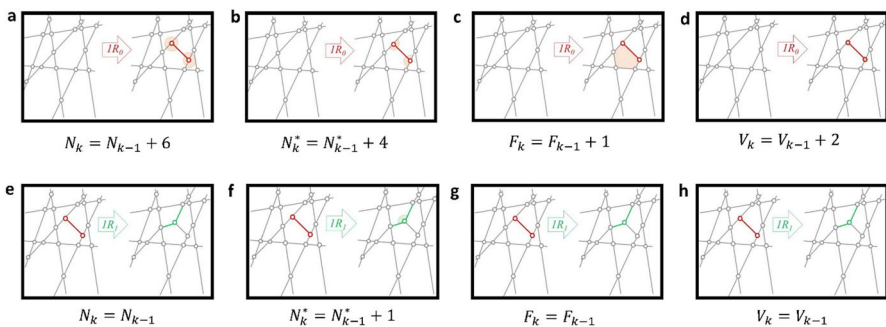


Fig. 3 Geometry of evolution steps R_0 and R_1 used in the model based on Hypothesis 1. In (a), (b), (c) and (d) we illustrate how step R_0 operates and in (e), (f), (g) and (h) we illustrate how R_1 operates on the fundamental quantities F, V, N, N^* of the tiling

Table 1 Evolutionary equations for the steps R_0 and R_1 used in the model based on Hypothesis 1

Step type	Name of the step	N_k	N_k^*	F_k	V_k
R_0	Secondary cracks	$N_{k-1} + 6$	$N_{k-1}^* + 4$	$F_{k-1} + 1$	$V_{k-1} + 2$
R_1	Crack healing rearrangement	N_{k-1}	$N_{k-1}^* + 1$	F_{k-1}	V_{k-1}

aforementioned variables. Table 1 shows eight recursion formulae of the type $x_k = f(x_{k-1})$ where the symbol x represents the fundamental quantities F, V, N, N^* . See also Fig. 3 for illustration.

Definition 11 Let M be a finite, convex, normal mosaic characterized by an initial state $(\bar{n}_1^*, \bar{v}_1^*)$ and let us denote by $(\bar{n}_p^*, \bar{v}_p^*)$ the limit point on the symbolic plane, reached after applying an infinite random sequence of R_0 and R_1 steps, with respective probabilities $1 - p, p$ and we call this a p -trajectory.

Remark 7 We mention two special p -trajectories: 0-trajectories correspond to sequences consisting entirely of R_0 -type steps and 1-trajectories correspond to sequences consisting entirely of R_1 -type steps. We also mention that the mosaics corresponding to any finite number of evolution steps R_0 and R_1 are, like the initial mosaic M , finite, convex, normal tilings. However, the limit point $(\bar{n}_p^*, \bar{v}_p^*)$ does not correspond to a normal mosaic, it should be regarded as a point of the symbolic plane.

The following lemma applies to general p -trajectories:

Lemma 1 Let M be a finite, normal, convex mosaic characterized by an initial state $(\bar{n}_1^*, \bar{v}_1^*)$. Then, for all p -trajectories we have $(\bar{n}_p^*, \bar{v}_p^*) = (\frac{4-3p}{2-2p}, \frac{4-3p}{1-p})$.

Proof

(a) After the first $c(1-p)$ steps of type R_0 we have:

$$N^*(c, p) = N_0^* + 4c(1 - p); F(c, p) = F_0 + c(1 - p); V(c, p) = V_0 + 2c(1 - p).$$

(b) After cp steps of type R_1 we have:

$$N^*(c, p) = N_0^* + cp; F(c, p) = F_0; V(c, p) = V_0.$$

Now we can compute limit for the mixed trajectory as c approaches infinity. Using (3) and (4) we can write:

$$\bar{n}_p^* = \lim_{c \rightarrow \infty} \bar{n}^*(c, p) = \lim_{c \rightarrow \infty} \frac{N_0^* + 4c(1 - p) + cp}{V_0 + 2c(1 - p)} = \frac{4 - 3p}{2 - 2p},$$

$$\bar{v}_p^* = \lim_{c \rightarrow \infty} \bar{v}^*(c, p) = \lim_{c \rightarrow \infty} \frac{N_0^* + 4c(1 - p) + cp}{F_0 + c(1 - p)} = \frac{4 - 3p}{1 - p}.$$

□

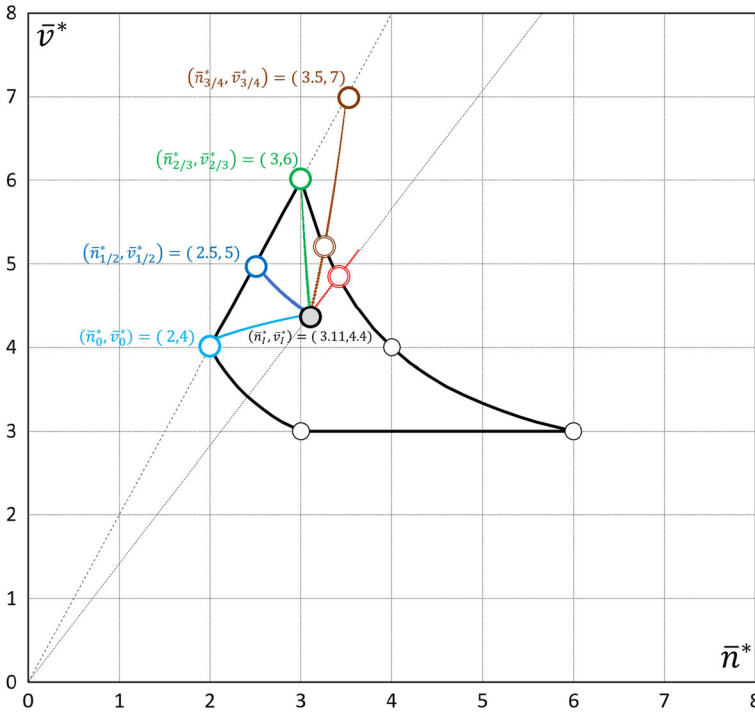


Fig. 4 Numerical simulation of p -trajectories on the symbolic plane. With initial mosaic at $(\bar{n}_I^*, \bar{v}_I^*) = (3.11, 4.4)$ (black circle with grey fill) we show 5 trajectories corresponding to $p = 0, 1/2, 2/3, 3/4, 1$, respectively. Limit points marked by colored circles with white interior. As predicted by Lemma 1, all limit points are on the $\bar{v}^* = 2\bar{n}^*$ line. Domain occupied by convex mosaics shown with black line, cf Domokos and Lángi (2019). Terminal points of physical trajectories marked by colored circles with double line. Dashed black lines correspond to $\bar{v}^* = 2\bar{n}^*$ and $\bar{v}^* = \bar{n}^* \bar{v}_I^* / \bar{n}_I^*$, respectively

The result of Lemma 1 is illustrated in Fig. 4 where we computed standard p -trajectories for $p = 0, \frac{1}{2}, \frac{2}{3}, \frac{3}{4}, 1$.

Remark 8 We can see that all limit points lie on the $\bar{v}^* = 2\bar{n}^*$ line. However, the *physically relevant* portion of the trajectory may terminate earlier. This is easiest understood if we consider the following argument: when constructing physically relevant p -trajectories we also have to consider Hypothesis 1, C(2) which implies that the necessary condition for an infinite p -trajectory to be physical is $p \leq 2/3$, as at least half as many R_0 steps are needed as we have R_1 steps. For $p \geq 2/3$, the physical part of the trajectory will terminate as the mosaic becomes regular at (or, for finite mosaics, near) the hyperbola defined in (5)(a). Beyond this point, the trajectory exists only in an algebraic sense (as a sequence of numbers) to which we do not attach any direct geometric interpretation. We also mention that, as $p \rightarrow 1$, the tangent of the trajectory at $(\bar{n}_I^*, \bar{v}_I^*)$ will approach the $\bar{\rho} = \text{constant}$ line with constant cell density passing through $(\bar{n}_I^*, \bar{v}_I^*)$, characterized by $\bar{v}^* = \bar{n}^* \bar{v}_I^* / \bar{n}_I^*$.

Remark 9 So far we described p -trajectories on finite domains and these trajectories appear on the symbolic plane as discrete point sequences. Based on Lemma 1, these sequences have limit points and the location of these points is independent of the initial point $(\bar{n}_I^*, \bar{v}_I^*)$, it just depends on the value of p . Now we extend this concept for the case where the initial mosaic is a balanced, infinite tiling M with averages $(\bar{n}_I^*(M), \bar{v}_I^*(M))$. We regard the limit process described in Definition 8: each finite value of the radius ρ defines a finite mosaic $M(\rho)$ and we have a p -trajectory on $M(\rho)$ with initial point $(\bar{n}_I^*(\rho), \bar{v}_I^*(\rho))$ and final point $(\bar{n}_p^*, \bar{v}_p^*)$, the latter being independent of ρ . Let us now regard a sequence of ρ approaching infinity. Then we have $\lim_{\rho \rightarrow \infty} (\bar{n}_I^*(\rho), \bar{v}_I^*(\rho)) = (\bar{n}_I^*(M), \bar{v}_I^*(M))$. We can run the same limit process after having executed a finite number of steps of a p -trajectory and after any finite number of steps we get convergence. So we can see that this process defines a sequence of trajectories which converge. We call the *limiting p -trajectory* with initial point $(\bar{n}_I^*(M), \bar{v}_I^*(M))$ and final point $(\bar{n}_p^*, \bar{v}_p^*)$ the p -trajectory associated with the infinite, balanced tiling M . We also note that trajectories corresponding to infinite tilings are represented in the symbolic plane by continuous line.

Needless to say, p -trajectories represent only a rather restricted class of geological evolution processes for fracture networks. In such a process, the ratio of R_0 -type and R_1 -type evolution steps remains constant. However, our model also admits statements of more general type.

Relying on Definitions 10 and 11 we make the following observation:

Lemma 2 *In the discrete-time fracture network evolution model formulated in Hypothesis 1, the cell density $\bar{\rho}(M)$ increases monotonically over time.*

Proof Since there are two steps in the model (R_0 and R_1), so, if we can show separately for both step-types that the cell density does not decrease, we have confirmed the statement of Lemma 2.

In the case of R_0 -type steps we have $N_{k_0}^* = N_{k_0-1}^* + 4; F_{k_1} = F_{k_1-1} + 1; V_{k_1} = V_{k_1-1} + 2$ (see Table 1) Note that from Definition 10 we have $\bar{\rho}(M) = \frac{V}{F}$, and we also note, based on (Domokos and Lángi 2019), that for any convex mosaic we have $\bar{\rho}(M) \leq 2$ (see also Remark 5). Based on these observations we see that cell density is increasing strictly monotonically under R_0 -type steps.

In the case of R_1 -type steps we have $N_{k_1}^* = N_{k_1}^* + 1; F_{k_2} = F_{k_2-1}; V_{k_2} = V_{k_2-1}$ (see Table 1), so here the cell density does not change.

As described above, in the crack network evolution model formulated in Hypothesis 1, the cell density is either constant or increasing in each step. □

So far, we did not make any additional restrictions on the initial mosaic M beyond requiring that it should be a convex, normal tiling. However, typical primary fracture networks have special position on the symbolic plane; in Domokos et al. (2020) it was argued that if the network is created by long straight fracture lines, then this corresponds to the point $(\bar{n}^*, \bar{v}^*) = (4,4)$ of the symbolic plane. Motivated by this geological observation we formulate.

Lemma 3 *In the discrete-time fracture network evolution model formulated in Hypothesis 1, if we choose an initial (starting) mosaic with $\bar{v}_I^*(M) < 4$ then the cell corner degree \bar{v}^* increases strictly monotonically over time.*

Proof Since there are two steps in the model (R_0 and R_1), so, if we can show separately for both that the cell corner degree increases in the case of an initial condition with $\bar{v}_l^*(M) < 4$, then we have confirmed the statement of Lemma 3.

In the case of R_0 -type steps we have $N_{k_0}^* = N_{k_0-1}^* + 4$; $F_{k_1} = F_{k_1-1} + 1$; $V_{k_1} = V_{k_1-1} + 2$ (see Table 1). Based on formula (4) we see that if in the initial state $\bar{v}_l^*(M) < 4$, \bar{v}^* will increase in the first step. Also, we have $\bar{v}^* < 4$ after any finite amount of steps and, as a consequence, \bar{v}^* is increasing strictly monotonically under R_0 type steps.

In the case of R_1 -type steps we have $N_{k_1}^* = N_{k_1}^* + 1$; $F_{k_2} = F_{k_2-1}$; $V_{k_2} = V_{k_2-1}$ (see Table 1), so, based on formula (4), here the cell corner degree \bar{v}^* is always increasing, regardless of the initial value. \square

4 Interpretation of the results and potential applications

Lemma 1 establishes the $\bar{v}^* = 2\bar{n}^*$ line as the global attractor for p -trajectories, i.e. for fracture pattern evolution processes where the relative weight of secondary fracture and crack healing/rearrangement remains constant over time. Our simple model represents crack pattern evolution in a constant environment. Geological evolution processes may be much more complex and so it appears to be feasible to approximate them piecewise by p -trajectories. All such general processes will ultimately converge onto a point of the $\bar{v}^* = 2\bar{n}^*$ line and this suggests that this line may have indeed significance, even beyond p -trajectories. This observation is underlined by Lemma 2 which states that cell density is growing monotonically over time. The $\bar{v}^* = 2\bar{n}^*$ line represents convex mosaics with maximal cell density $\bar{\rho}(M) = 2$.

Since cell density evolves monotonically, it defines a hierarchy among fracture patterns. This hierarchy may be defined even more sharply by connecting mosaics with a p -trajectory; however, this may not always be possible. In this respect we formulate.

Conjecture 1 *Let M_1 and M_2 be two infinite, convex, balanced mosaics. Then, in this model, they can be related two different ways: Either there exists a unique value $0 \leq p(M_1, M_2) \leq 1$ such that a unique p -trajectory connects M_1 and M_2 or there is no p -trajectory connecting M_1 and M_2 .*

In the first case we can say that M_1 and M_2 are p -related, in the second case we say that M_1 and M_2 are unrelated in the model. While these considerations are neither entirely rigorous nor are they supported by experiments, our model and the results derived from this model suggest that the *maturity* of a fracture network may be related to the cell density $\bar{\rho}(M)$ of the convex mosaic representing it.

In Fig. 5 we show two mud crack patterns (discussed in detail in Domokos et al. (2020), shown in Fig. 1a, b of the current article) connected by a $p = 0.685$ trajectory in the (b) \rightarrow (a) direction. While this connection certainly does not indicate that pattern (a) evolved from pattern (b), it does tell us that the inverse would not be compatible with the model and this might help a meaningful geological comparison. We also remark that desiccation would suggest an opposite evolution, however, that would certainly not produce an exact (a) \rightarrow (b) trajectory. The existence of a trajectory in

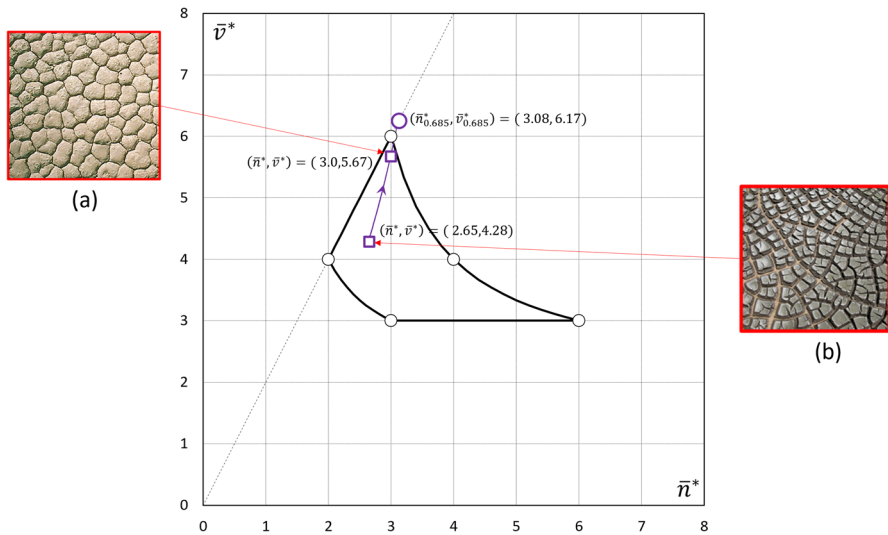


Fig. 5 Mud crack patterns shown in Fig. 1a, b of this paper [from Fig. 3 in Article (Domokos et al. 2020)], connected by a $p = 0.685$ trajectory in the direction (b) \rightarrow (a)

the opposite direction suggests that in a wet environment this evolution could possibly take place.

Acknowledgements The authors thank Marjorie Senechal and two anonymous referees for the discussion and helpful comments. The support of the NKFIH Hungarian Research Fund Grant 134199 and of the NKFIH Fund TKP2021 BME-NVA, carried out at the Budapest University of Technology and Economics, is kindly acknowledged. Krisztina Regős: This research has been supported by the program ÚNKP-22-3 by ITM and NKFIH. The gift representing the Albrecht Science Fellowship is gratefully appreciated.

Funding Open access funding provided by Budapest University of Technology and Economics.

Open Access This article is licensed under a Creative Commons Attribution 4.0 International License, which permits use, sharing, adaptation, distribution and reproduction in any medium or format, as long as you give appropriate credit to the original author(s) and the source, provide a link to the Creative Commons licence, and indicate if changes were made. The images or other third party material in this article are included in the article's Creative Commons licence, unless indicated otherwise in a credit line to the material. If material is not included in the article's Creative Commons licence and your intended use is not permitted by statutory regulation or exceeds the permitted use, you will need to obtain permission directly from the copyright holder. To view a copy of this licence, visit <http://creativecommons.org/licenses/by/4.0/>.

References

- Adler PM, Thovert JF (1999) Fractures and fracture networks. Springer, Dordrecht
- Aydin A, DeGraff JM (1988) Evolution of polygonal fracture patterns in lava flows. *Science* 239(4839):471–476
- Bird P (2003) An updated digital model of plate boundaries. *Geophys Geochem Geosyst* 4(3):1–52. <https://doi.org/10.1029/2001GC000252>

- Domokos G, Horváth ÁG, Regős K (2022) A two-vertex theorem for normal tilings. *Aequat Math*. <https://doi.org/10.1007/s00010-022-00888-0>
- Domokos G, Jerolmack DJ, Kun F, Török J (2020) Plato's cube and the natural geometry of fragmentation. *Proc Natl Acad Sci* 117(31):18178–18185
- Domokos G, Lángi Z (2019) On some average properties of convex mosaics. *Exp Math*. <https://doi.org/10.1080/10586458.2019.1691090>
- García-Rodríguez M (2015) Polygonal cracking associated to vertical and subvertical fracture surfaces in granite (La Pedriza del Manzanares, Spain): considerations for a morphological classification. *J Iber Geol* 41(3):365–383
- Goehring L (2013a) Evolving fracture patterns: columnar joints, mud cracks and polygonal terrain. *Philos Trans R Soc A* 371:20120353
- Goehring L, Morris SW (2008) Scaling of columnar joints in basalt. *J Geophys Res Solid Earth*. <https://doi.org/10.1029/2007JB005018>
- Goehring L, Nakahara A, Dutta T, Kitsunozaki S, Tarafdar S (2015) Desiccation cracks and their patterns: formation and modeling in science and nature. Wiley, New York
- Grünbaum B, Shepard GC (1987) Tilings and patterns. Freeman and Co., New York
- Jagla EA, Rojo AG (2002) Sequential fragmentation: the origin of columnar quasihexagonal patterns. *Phys Rev E* 65(2):026203
- Ma X, Lowensohn J, Burton JC (2019) Universal scaling of polygonal desiccation crack patterns. *Phys Rev* 99:012802
- Nagle-McNaughton TP (2021) Scuderi, LA Networked configurations as an emergent property of transverse aeolian ridges on Mars. *Commun Earth Environ* 2:217. <https://doi.org/10.1038/s43247-021-00286-5>
- Peacock DCP, Sanderson DJ, Rotevatn A (2018) Relationships between fractures. *J Struct Geol* 106:41–53
- Schattschneider D, Senechal M (2004) Tilings Chapter 3. In: Goodman J, O'Rourke J (eds) *Discrete and computational geometry*. CRC Press, Boca Raton
- Schneider R, Weil W (2008) *Stochastic and integral geometry*. Springer, Berlin
- Stacey S, Sammis C (1991) An automaton for fractal patterns of fragmentation. *Nature* 353:250–252
- Turcotte DL (1986) Fractals and fragmentation journal of geophysical research/solid. *Earth* 91(B2):1921–1926
- Vrankic I, Herceg T, Bach MP (2021) Dynamics and stability of evolutionary optimal strategies in duopoly. *CEJOR* 29:1001–1019. <https://doi.org/10.1007/s10100-020-00713-6>

Publisher's Note Springer Nature remains neutral with regard to jurisdictional claims in published maps and institutional affiliations.